Control and Performance of Capacitively-Isolated Bidirectional DC-DC Converter with Auxiliary Converters for Electric Railways

Kana Matsumoto[1*], Kazuaki Tesaki[1], Makoto Hagiwara[1]
1 Electrical and Electronic Engineering, Tokyo Institute of Technology, Tokyo, Japan
*E-mail: matsumoto.k.bo@m.titech.ac.jp

***Abstract*—This paper presents the operating principles and control methods of a capacitively-isolated bidirectional dc-dc converter with auxiliary converters, which is intended for high power applications. It consists of a main converter, two auxiliary converters, two inductors, and two isolation capacitors. The proposed converter is characterized by achieving galvanic insulation and isolation without using transformer. In addition, it can achieve robust bidirectional power-flow control using the auxiliary converters. Further, the proposed converter can eliminate dc circuit breakers from the circuit. The operating principles and control methods presented in this paper are verified by experiments using a 200-W, 75-V down-scaled model.**

***Keywords*—capacitive galvanic isolation, dc-dc converter.**

I. Introduction

Electric railway is one of the mass public transportation systems that can achieve the reduction of carbon dioxide emissions [1], and it is an effective means for solving global warming. In recent years, many research and development intended for further energy savings of electrical vehicles have been carried out using state-of-the-art power electronics technologies.

The line-frequency transformer (LFT) is widely applied to the railway traction systems fed by the catenary having medium voltage and low line frequency (e.g., 25 kV/60 Hz [1] 15 kV/16.7 Hz [2] and 25 kV/50 Hz [3]), which is responsible for voltage insulation and isolation and step-down of the catenary voltage. Meanwhile, it suffers from the disadvantage of large mass and volume because it operates under the line frequency of 16.7, 50, or 60 Hz. According to [4], the mass of LFTs is up to 4 tons. Therefore, the elimination of the LFTs is indispensable to achieve energy savings of railway vehicles.

To achieve this aim, numerous circuit topologies have been studied. The authors [5], [6], [7], [8], [9] have shown the circuit topologies called the dual-active-bridge (DAB) converters [5], [6], [7] and resonant LLC converters [8], [9]. These circuits are characterized by achieving the soft switching (i.e., zero-current switching or zero-voltage switching) of power devices, which results in volume reduction of transformers owing to the increased switching frequency. However, the downsizing of transformers is limited because the thermal management of the high-frequency transformer is difficult. Moreover, the optimum transformer design is complicated [6], [10]. The authors [4], [11] have focused on the circuit topology based on the switched-capacitor converters capable of semiconductor-based galvanic isolation (SGI). The purpose of SGI is to achieve high power density by replacing transformers with capacitors. However, the capacitor voltage control was not implemented in [4] and power flow control was achieved by feedforward control, which results in a system vulnerable to disturbances. Moreover, external dc-circuit breakers are indispensable for protecting the system when power devices fail.

This paper presents the operating principles and control methods of a capacitively-isolated bidirectional dc-dc converter with auxiliary converters, which is intended for high power applications. It consists of a main converter, two auxiliary converters, two inductors, and two isolation capacitors. The proposed converter is characterized by achieving galvanic insulation and isolation between the high- and low-voltage sides without using transformers. In addition, it can achieve robust bidirectional power-flow control using the auxiliary converters. Moreover, the proposed converter can eliminate dc circuit breakers from the system because the isolation capacitors work as a dc-circuit breaker. The operating principles and control methods presented in this paper are verified by experiments using a 200-W, 75-V down-scaled model.

II. Circuit Configuration and Advantage

A. Circuit Configuration

Fig. 1(a) shows the circuit configuration of the proposed capacitively-isolated bidirectional dc-dc converter which consists of a main converter, two auxiliary converters, two isolation capacitors, and two inductors. V_{dc1} and V_{dc2} are the high- and low-voltage-side voltages, and i_{dc1} and i_{dc2} are the high- and low-voltage-side currents, respectively. The main converter is formed of four power devices, S_1, S_2, S_3, and S_4, where it acts as a voltage-source converter. v_{S1} and v_{S2} are the voltages of S_1 and S_2. The dc-link capacitors, C_{f1} and C_{f2}, are inserted between two voltage sources as shown in Fig. 1(a). Specifically, the isolation capacitors are connected between S_1 and S_2 as well as S_3 and S_4. They are responsible for galvanic isolation between the high- and low-voltage sides, and the same technique is used in the conventional capacitively-isolated converters [12]. v_{C1}, v_{C2}, i_{C1}, and i_{C2} represent the voltages and the currents of each isolation capacitor. Fig. 1(b) shows the circuit

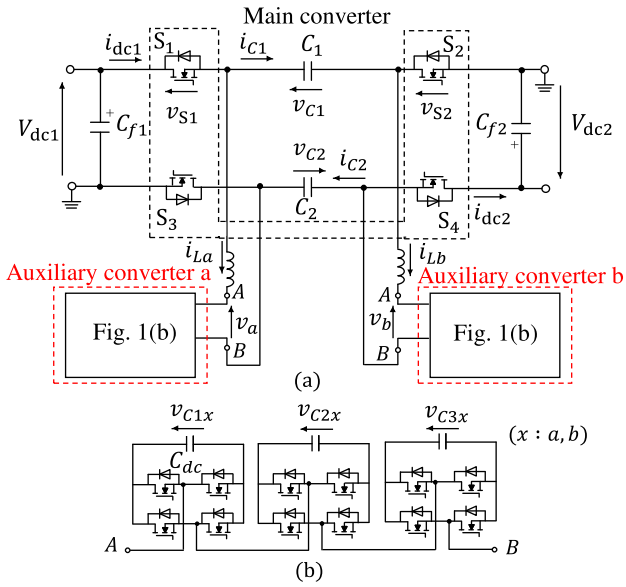

Fig. 1. Circuit configuration of the capacitively-isolated bidirectional dc-dc converter. (a) Overall configuration. (b) Auxiliary converter.

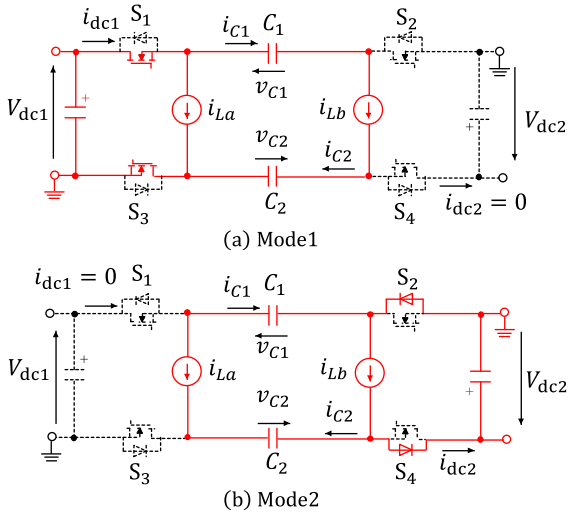

Fig. 2. Two operating modes of Fig. 1 according to the switching states. (a) Mode 1. (b) Mode 2.

configuration of the auxiliary converter. v_{C1x}, v_{C2x}, and v_{C3x} are capacitor voltage of each bridge cell , C_{dc} is dc-capacitors in the auxiliary converters. It is based on the cascade connection of multiple bridge cells (i.e., single-phase full-bridge or H-bridge converters), and it is connected to the main converter via an inductor L. The combination of an inductor and an auxiliary converter works as a robust controlled current source.

B. Advantage of Fig. 1 over Conventional Circuit

A capacitively-isolated dc-dc converter based on half-bridge resonant circuit has been studied in [12], which uses two isolation capacitors as Fig. 1(a). A common-mode current flows in the circuit when the negative terminals of supply and load sides are grounded, which means that the galvanic insulation cannot be maintained. Meanwhile, the Fig. 1 circuit can maintain the galvanic insulation even when the negative terminals of supply and load (or another supply) sides are grounded because the main converter has the function of blocking the common-mode current by switching S_1 (S_3) and S_2 (S_4) complementarily.

III. Principles of Operation

To simplify the analysis, the dead time of both main and auxiliary converters is set to zero, and the parasitic resistance, parasitic inductance, voltage drops of L, and converter losses are assumed to be zero. Moreover, the combination of inductor and auxiliary converter is assumed to be a current source producing i_{La} (> 0) or i_{Lb} (> 0).

Fig. 2 shows two operating modes of Fig. 1 according to the switching states of the main converter, where the power is sent from high-voltage side to low-voltage side. The pair of S_1 and S_3 and that of S_2 and S_4 turns on/off complementarily. In mode 1 where S_1 (S_3) is on and

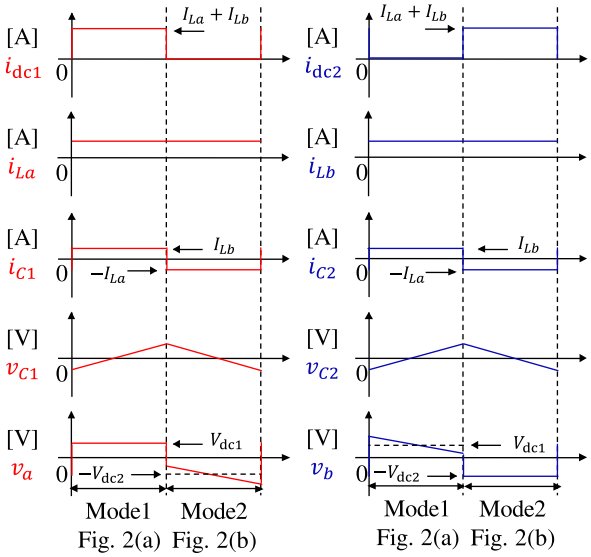

Fig. 3. Ideal voltage and current waveforms of Fig. 1 when the power is sent from high-voltage side to low-voltage sides.

S_2 (S_4) is off, the current flows to S_1 and S_3, and the power is sent from V_{dc1} to dc-capacitors in the auxiliary converters as shown in Fig. 2(a). In mode 2 where S_1 (S_3) is off and S_2 (S_4) is on, the current flows to S_2 and S_4, and the power is sent from dc-capacitors in the auxiliary converters to V_{dc2} as shown in Fig. 2(b). The proposed converter is capable of bidirectional power transmission using the electrostatic energy of dc-capacitors in the auxiliary converters where the operation is similar to that of traditional switched capacitor converters.

A. Basic Operation of Main Converter

Fig. 3 shows the ideal voltage and current waveforms of Fig. 1. From Fig. 2(a), the following equations hold in

mode 1:

$$i_{\mathrm{dc1}} = i_{La} + i_{Lb}, \tag{1}$$
$$i_{C1} = i_{C2} = i_{Lb}. \tag{2}$$

The one-period average power transmitted from high-voltage side to auxiliary converters, P_{dc1}, is obtained from (1) as

$$P_{\mathrm{dc1}} = dV_{\mathrm{dc1}}(i_{La} + i_{Lb}), \tag{3}$$

where d is the duty ratio of S_1 (S_3). Similarly, the following equation holds in mode 2:

$$i_{\mathrm{dc2}} = i_{La} + i_{Lb}, \tag{4}$$
$$i_{C1} = i_{C2} = -i_{La}. \tag{5}$$

The one-period average power transmitted from the auxiliary converters to the low-voltage side, P_{dc2}, is obtained from (4) as

$$P_{\mathrm{dc2}} = (1-d)V_{\mathrm{dc2}}(i_{La} + i_{Lb}). \tag{6}$$

The relationship $P_{\mathrm{dc1}} = P_{\mathrm{dc2}}$ holds under steady states. Based on (3) and (6), d is determined by the following equation:

$$d = \frac{V_{\mathrm{dc2}}}{V_{\mathrm{dc1}} + V_{\mathrm{dc2}}}. \tag{7}$$

Equation (7) means that d is the same as the one applied to the conventional buck-boost converter. It should be noted that an additional component is superimposed in (7) for regulating the dc-capacitor voltages used in the auxiliary converters as shown in Fig. 4.

B. Basic Operation of Auxiliary Converter

The auxiliary converter acts as a controlled current source and regulates the inductor current i_{Lx} to a dc reference. In mode 1 (Fig. 2(a)), the following equation holds for the auxiliary converter output voltages v_a and v_b.

$$v_a = V_{\mathrm{dc1}}, \tag{8}$$
$$v_b = V_{\mathrm{dc1}} - v_{C1} - v_{C2}, \tag{9}$$
$$v_x > 0,\ i_{Lx} > 0\ (x \ni a, b). \tag{10}$$

From (10), the instantaneous power p_a ($= v_a i_{La}$) and p_b ($= v_b i_{Lb}$) are always positive. In other words, the power supplied by V_{dc1} is charged to the dc-capacitors in the auxiliary converter as an electrostatic energy. Meanwhile, In mode 2 (Fig. 2(b)), the following equation holds for the auxiliary converter output voltages v_a and v_b.

$$v_a = -V_{\mathrm{dc2}} + v_{C1} + v_{C2}, \tag{11}$$
$$v_b = -V_{\mathrm{dc2}}, \tag{12}$$
$$v_x < 0,\ i_{Lx} > 0\ (x \ni a, b). \tag{13}$$

From (13), the instantaneous power p_a and p_b of are always negative and the electrostatic energy stored in the dc-capacitors in the auxiliary converter is transmitted to V_{dc2}.

Focusing on the auxiliary converter output voltages v_a and v_b and inductor currents i_{La} and i_{Lb} in Fig. 3 reveals that v_a and v_b are composed of ac components, while i_{La} and i_{Lb} are composed of dc components. Therefore, the instantaneous power (p_a, p_b) that flows in and out of the auxiliary converters are composed of the ac component. As a result, only ac power is supplied to each bridge cell without any dc power. In other words, the dc-capacitor voltages of the auxiliary converter can be regulated to a constant value because the one-period average power is zero. However, the voltage control should be applied to the axillary converter to compensate power loss in the converter, and the individual and voltage balancing control, which will be mentioned later, should be applied.

C. Isolation Capacitors

Isolation capacitors are intended to separate conductors between V_{dc1} and V_{dc2}. In mode 1 (Fig. 2(a)), the isolation-capacitor voltages v_{C1} and v_{C2} are given by the following equations from (2).

$$v_{C1} = \frac{1}{C_1}\int i_{C1}\,dt = \frac{1}{C_1}\int i_{Lb}\,dt, \tag{14}$$
$$v_{C2} = \frac{1}{C_2}\int i_{C2}\,dt = \frac{1}{C_2}\int i_{Lb}\,dt. \tag{15}$$

Assuming that the dc component of i_{Lb} is I_{Lb} in (14) and (15), v_{C1} and v_{C2} increase linearly with the slope $\frac{I_{Lb}}{C_1}$ or $\frac{I_{Lb}}{C_2}$. Meanwhile, In mode 2 (Fig. 2 (b)), the isolation-capacitor voltages v_{C1} and v_{C2} are given by the following equations from (5).

$$v_{C1} = \frac{1}{C_1}\int i_{C1}\,dt = -\frac{1}{C_1}\int i_{La}\,dt, \tag{16}$$
$$v_{C2} = \frac{1}{C_2}\int i_{C2}\,dt = -\frac{1}{C_2}\int i_{La}\,dt. \tag{17}$$

Assuming that the dc component of i_{La} is I_{La} in (16) and (17), v_{C1} and v_{C2} decrease linearly with the slope $-\frac{I_{La}}{C_1}$ or $-\frac{I_{La}}{C_2}$. In order to regulate the dc components of v_{C1} and v_{C2} constant, it is necessary to control the one-period average of the isolated-capacitor currents i_{C1} and i_{C2} to zero. In order to realize the above, it is necessary to satisfy the following equation regarding the inductor currents i_{La} and i_{Lb} as

$$i_{Lb} = \frac{V_{\mathrm{dc1}}}{V_{\mathrm{dc2}}} i_{La}. \tag{18}$$

When (18) holds, the amount of increase and that of decrease are equal, and the dc components in v_{C1} and v_{C2} are kept constant. When i_{Lb} is larger than the value given by (18), the amount of slope increase exceeds the amount of slope decrease, so that the dc components in v_{C1} and v_{C2} increase. Meanwhile, when i_{Lb} is smaller than the value given by (18), the amount of slope decrease exceeds the amount of slope increase, so the dc components in v_{C1} and v_{C2} decrease. The above relationship can be used to control the sum of v_{C1} and v_{C2}.

IV. Control Methods

The following focuses on the control method of Fig. 1 where the bridge cell count is $N = 3$.

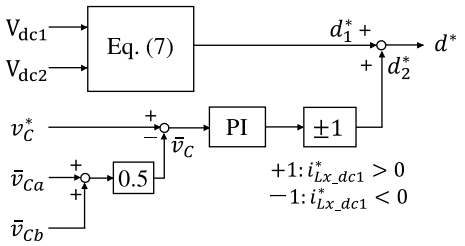

Fig. 4. Block diagram for main converter control.

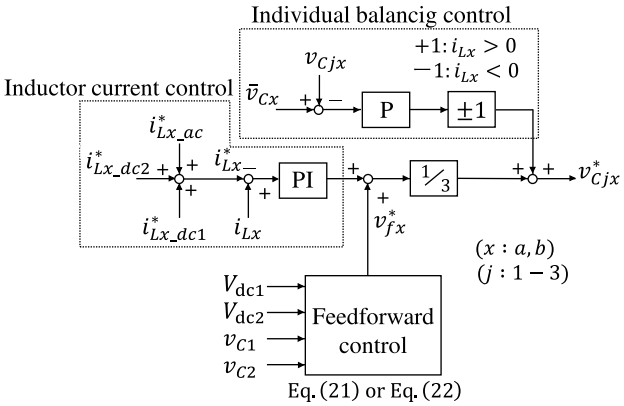

Fig. 5. Block diagram for auxiliary converters control.

A. Main Converter Switching

The reference value for the duty ratio of the main converter, d^*, is the sum of feedforward component, d_1^*, and feedback component, d_2^* ($d^* = d_1^* + d_2^*$). The former is calculated from (7) using $V_{\rm dc1}$ and $V_{\rm dc2}$ detected by voltage sensors. The latter is calculated from the feedback control of all the dc-capacitor voltages used in the auxiliary converters. Specifically, the arithmetic average value of all the dc-capacitor voltages used in the auxiliary converters, $\overline{v}_C$, is regulated to a reference value, v_C^*, using the conventional PI control, producing d_2^*.

B. Auxiliary Converters Control System

Fig. 5 shows the control block diagram for the auxiliary converters, where it is divided into the following three controls:

- Inductor current control;
- Feedforward control;
- Individual balancing control.

1) Inductor current control: Inductor current control forms a feedback loop between the inductor current i_{Lx} and the current reference value i_{Lx}^* based on the conventional PI control. Further, this control can be classified into the following three sub-controls:

- Voltage balancing control of dc-capacitors used in the auxiliary converters;
- Power-flow control;
- Voltage control of isolation capacitors.

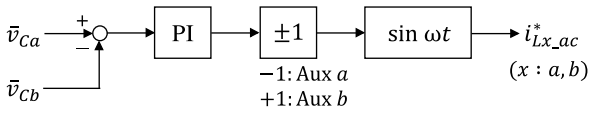

Fig. 6. Block diagram for voltage balancing control of dc-capacitor voltages used in the auxiliary converters.

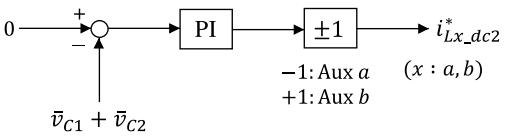

Fig. 7. Block diagram for voltage control of isolated capacitors.

Fig. 6 shows the block diagram for voltage balancing control of dc-capacitor voltages used in the auxiliary converters. It is achieved by superimposing an ac component with the frequency of $f_{\rm CM}$, which is the switching frequency of the main converter, into the inductor currents i_{La} and i_{Lb}. In Fig. 6 , $\overline{v}_{Cx}$ $(x : a, b)$ is the arithmetic average voltage of the dc-capacitor voltages, which is given by

$$\overline{v}_{Cx} = \frac{1}{3}(v_{C1x} + v_{C2x} + v_{C3x}). \tag{19}$$

The conventional PI control is used for achieving the relationship $\overline{v}_{Ca} = \overline{v}_{Cb}$ where the output of the PI controller is different in each auxiliary converter as shown in Fig. 6. Subsequently, the output of the PI controller is multiplied by $\sin\omega t = \sin 2\pi f_{\rm CM} t$, producing the current reference, $i^*_{Lx\_ac}$. It should be noted that $i^*_{Lx\_ac}$ corresponds to a circulating current flowing between the auxiliary converters and isolation capacitors. For example, when $\overline{v}_{Ca} > \overline{v}_{Cb}$, the power is flowing out from the auxiliary converter a, and the same power is flowing into the auxiliary converter b using $i^*_{Lx\_ac}$. A similar technique is used in modular multilevel cascade converters.

The power-flow control is responsible for power control between $V_{\rm dc1}$ and $V_{\rm dc2}$, and controls the amount of dc components in each inductor current i_{Lx}. The same relationship as shown in (18) holds between the current reference value $i^*_{La\_dc1}$ of the auxiliary converter a and the current reference value $i^*_{Lb\_dc1}$ of the auxiliary converter b. From equations (3), (6), (7) and (18), $P_{\rm dc1}$ and $P_{\rm dc2}$ can be transformed into the following equation.

$$P_{\rm dc1} = P_{\rm dc2} = V_{\rm dc1} I_{La} = V_{\rm dc2} I_{Lb}. \tag{20}$$

Fig. 7 shows the block diagram for voltage control of isolation capacitors. This control is realized by feedback control of the sum of two isolation-capacitor voltages. Specifically, the current reference $i^*_{Lx\_dc2}$ is used for the voltage control, which is based on the feedback control of $\overline{v}_{C1} + \overline{v}_{C2}$ and the reference value of zero as shown in Fig. 7. It should be noted that an moving-average filter of $f_{\rm CM}$ is applied to v_{C1} and v_{C2} to detect only the dc components. Further, the polarity of the output of the PI controller is changed for each auxiliary converter. It

TABLE I. CIRCUIT PARAMETERS OF FIG. 1 USED IN EXPERIMENTS.

Rated power	P	200 W
High-side voltage	$V_{\rm dc1}$	75 V
Low-side voltage	$V_{\rm dc2}$	75 V
Dc capacitor voltage	V_C	35 V
Bridge cell count	N	3
Carrier freq. (Main)	$f_{\rm CM}$	500 Hz
Carrier freq. (Aux.)	$f_{\rm CA}$	4 kHz
Equivalent carrier freq.	$Nf_{\rm CA}$	24 kHz
Inductor	L	0.75 mH (8.3%)
Isolation capacitor	C_1, C_2	1 mF
Dc capacitor	C_{dc}	6 mF
Dc-link capacitor	C_{f1}, C_{f2}	3.3 mF
Dead time	$T_{\rm D}$	3.2 μs

Value in () is on a 75-V, 200-W, and 500-Hz base.

should be noted that it is impossible to control $\overline{v}_{C1}$ and $\overline{v}_{C2}$ independently.

2) Feedforward control: The feedforward control serves to remove the main converter carrier frequency component of $f_{\rm CM}$ contained in the inductor current i_{Lx}. Consequently, the ripple current and inductance can be reduced. The feedforward voltage reference values v^*_{fa} and v^*_{fb} of the following equations are given to each auxiliary converter depending on each mode.

$$v^*_{fa} = \begin{cases} V_{\rm dc1} & ({\rm S}_1 : {\rm on}, {\rm S}_2 : {\rm off}) \\ -V_{\rm dc2} + v_{C1} + v_{C2} & ({\rm S}_1 : {\rm off}, {\rm S}_2 : {\rm on}), \end{cases} \quad (21)$$

$$v^*_{fb} = \begin{cases} V_{\rm dc1} - v_{C1} - v_{C2} & ({\rm S}_1 : {\rm on}, {\rm S}_2 : {\rm off}) \\ -V_{\rm dc2} & ({\rm S}_1 : {\rm off}, {\rm S}_2 : {\rm on}). \end{cases} \quad (22)$$

3) Individual balancing control: The individual balancing control achieves voltage balance by forming active power between each bridge cell output voltage and inductor current. Specifically, feedback control is performed with $\overline{v}_{Cx}$ in (19) and the instantaneous value v_{Cjx} of each dc-capacitor voltage, and active power is exchanged between each cell. The polarity of the voltage reference value should be changed according to that of i_{Lx}.

V. EXPERIMENT

A. Experimental Conditions

A 200-W, 75-V down-scaled model is used for the verification of Fig. 1. Table I summarizes the circuit parameters used in experiments. Si-MOSFETs were used as power devices in the main converter and SiC-MOSFETs were used as power devices in the auxiliary converters. The high-voltage-side dc voltage was $V_{\rm dc1} = 75$ V, and the low-voltage-side dc voltage was $V_{\rm dc2} = 75$ V. The film capacitors were applied to the isolation capacitors, and the capacitance was $C_1 = C_2 = 1$ mF. The dc-capacitor voltage of the bridge cell was $V_C = 35$ V, and the capacitance of the bridge cell was set to $C_{\rm dc} = 6$ mF. The capacitance of dc-link capacitors was set to 3.3 mF. The carrier frequency of the main converter was set to $f_{\rm CM} = 500$ Hz, and that of the bridge cell in the auxiliary converter was set to $f_{\rm CA} = 4$ kHz. The dead time of both converters was set to $T_{\rm D} = 3.2$ μs. The inductance was

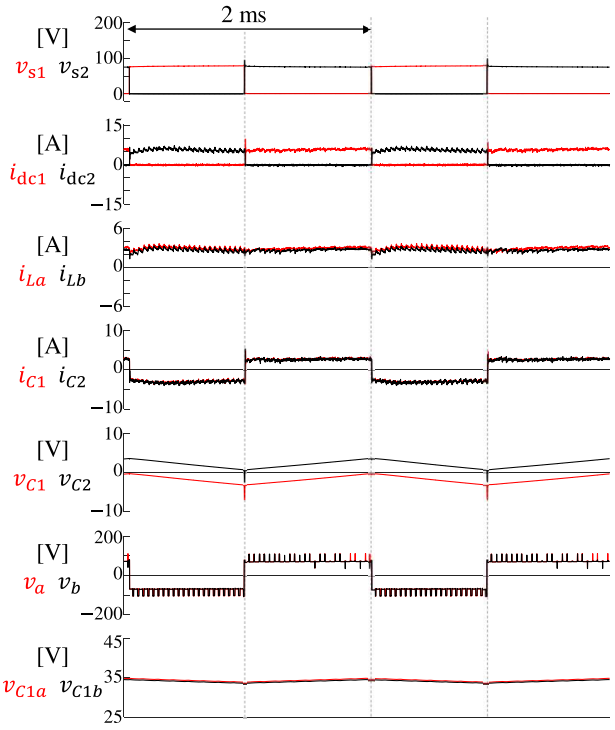

Fig. 8. Experimental waveforms when $V_{\rm dc1} = 75$ V, $V_{\rm dc2} = 75$ V, and $P = 200$ W, where the power was sent from high-voltage side to low-voltage side.

$L = 0.75$ mH, and the percent impedance is 8.3% based on P, $V_{\rm dc1}$, and $f_{\rm CM}$.

NF's programmable ac power supply DP series typeR (DP030RS) is used for the dc power supply on the high-voltage side and low-voltage side. The control system consists of a digital signal processor (DSP) unit using the Texas Instruments TMS320C6678 and a field-programmable gate array (FPGA) unit using the Altera Cyclone IV. The FPGA unit including A/D converters detects the six dc-capacitor voltages of each bridge cell, the two isolation-capacitor voltages, the two inductor currents, and the high- and the low-side dc voltages. The FPGA unit produces 28-bit gate signals in total. The Tektronix oscilloscope DPO4034B (frequency band: 2.5 GHz) and MDO41404C (frequency band: 5 GHz) were used to measure the current waveforms, and the Hioki Memory HiCorder MR6000-01 (frequency band: 30 MHz) was used to measure the voltage waveforms. The experimental "current" waveforms were captured using the Tektronix (TCP0020) with a frequency band of 50 MHz, the Tektronix (TCP0150) with a frequency band of 20 MHz, the Tektronix (TCP305a) with a frequency band of 50 MHz, and the Tektronix (TCP303) with a frequency band of 15 MHz.

B. Experimental Results

Fig. 8 shows experimental waveforms when $V_{\rm dc1} = 75$ V, $V_{\rm dc2} = 75$ V, and $P = 200$ W, where the power was sent from high-voltage side to the low-voltage side and current waveforms correspond to those shown in Fig. 1(a).

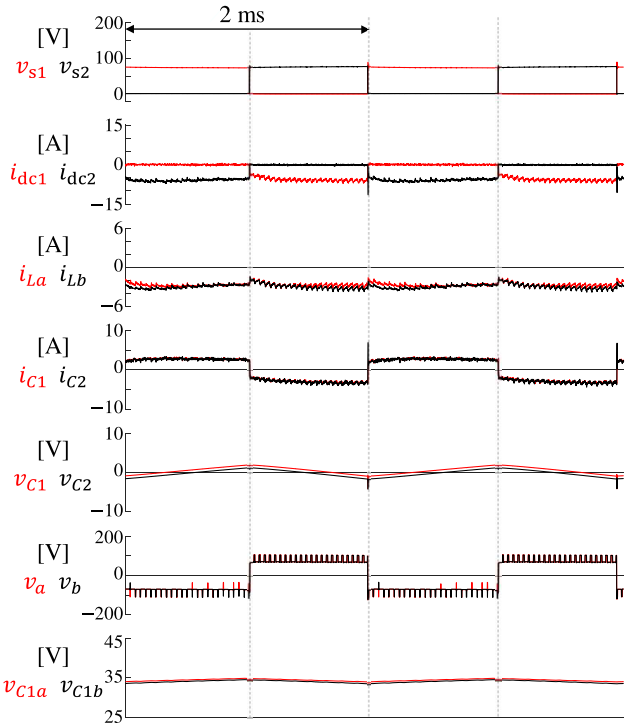

Fig. 9. Experimental waveforms when $V_{\rm dc1} = 75$ V, $V_{\rm dc2} = 75$ V, and $P = 200$ W, where the power was sent from low-voltage side to high-voltage side.

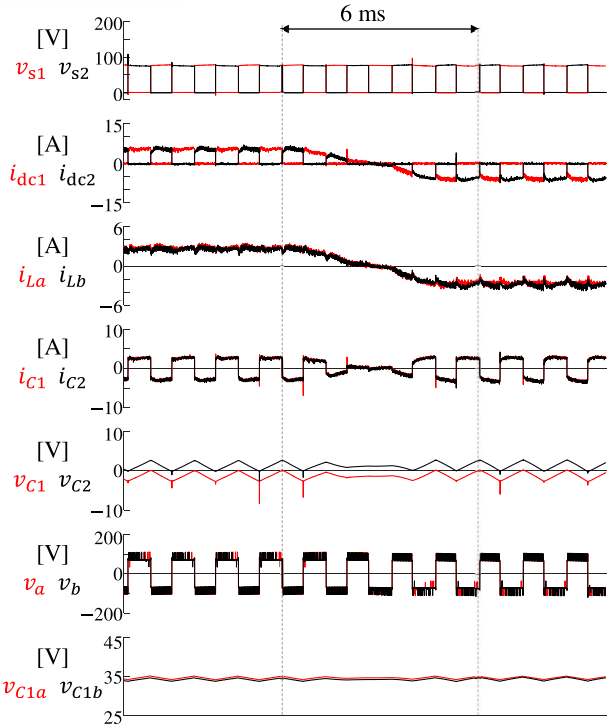

Fig. 10. Experimental waveforms when $V_{\rm dc1} = 75$ V, $V_{\rm dc2} = 75$ V, where the direction of the power flow is reversed in 6 ms.

The main converter turned on/off complementarily with a duty ratio of about 0.5 based on (7). The actual duty ratio is different from 0.5 because of d_2^* in Fig. 4. The high- and low-voltage-side currents, $i_{\rm dc1}$ and $i_{\rm dc2}$, are square-wave currents, where they are the sum of i_{La} and i_{Lb}. The inductor currents, i_{La} and i_{Lb}, contain a dc component, a 500 Hz ac component that is equal to the carrier frequency of the main converter, and a 24 kHz switching ripple component. It can be seen that each dc component in i_{La} and i_{Lb} is slightly different in amplitude to regulate the average value of the isolation-capacitor voltages to zero. The isolation capacitor currents i_{C1} and i_{C2} are square waves equal to i_{Lb} in mode 1 and equal to $-i_{La}$ in mode 2, depending on the switching state of the main converter. The isolation-capacitor voltages, v_{C1} and v_{C2}, included a 500 Hz ac component, and the dc component of $v_{C1} = -1.8$ V, v_{C2} =2.1 V. The reason for this interesting phenomenon originates from losses in the isolation capacitors. The voltages of the auxiliary converters, v_a and v_b, are seven-level waveforms with a voltage step of 35 V ($= V_C$) owing to the phase-shifted PWM. Each voltage is the sum of voltage components produced by inductor current control, feedforward control and individual balancing control. In addition, 24 kHz switching-ripple voltages are included. The dc-capacitor voltages v_{C1a} and v_{C1b} show that their dc components are well regulated to the reference value of 35 V. They also contain a 500 Hz ac component with $f_{\rm CM}$, and an 8 kHz switching ripple component. However, the ac component and the switching ripple component are sufficiently smaller than the dc component.

Fig. 9 shows the experimental waveforms when $V_{\rm dc1} = 75$ V, $V_{\rm dc2} = 75$ V, and $P = 200$ W, where the power was sent from low-voltage side to high-voltage side. A comparison of Fig. 8 and Fig. 9 shows that both waveforms are similar except for the polarity of the following currents: i_{La}, i_{Lb}, $i_{\rm dc1}$, $i_{\rm dc2}$, i_{C1}, and i_{C2}. The dc-capacitor voltages v_{C1a} and v_{C1b} show that their dc components are well regulated to the reference value of 35 V.

Fig. 10 shows the experimental waveforms when $V_{\rm dc1} = 75$ V, $V_{\rm dc2} = 75$ V, where the direction of the power flow is reversed in 6 ms. It was confirmed that even when the power-flow direction was transiently changed in 6 ms, no overvoltage or overcurrent occurred in each current/voltage waveform.

VI. Conclusions

This paper has proposed a capacitively-isolated bidirectional dc-dc converter with auxiliary converters. It is characterized by achieving galvanic insulation and isolation between the high- and low-voltage sides without using transformer. The validity and effectiveness of the control method were confirmed by experimental verification using a 200-W, 75-V down-scaled model.

REFERENCES

[1] H. Hayashiya et al, "Review of Regenerative Energy Utilization in Traction Power Supply System in Japan: Applications of Energy Storage Systems in d.c. Traction Power Supply System," *IECON 2017 - 43rd Annual Conference of the IEEE Industrial Electronics Society,* pp. 3918–3923, 2017.

[2] M. Steiner and H. Reinold, "Medium Frequency Topology in Railway Applications," *2007 European Conference on Power Electronics and Applications,* pp. 1–10, 2007.

[3] M. Mermet-Guyennet, "New Power Technologies for Traction Drives," *SPEEDAM 2010,* pp. 719–723, 2010.

[4] T. Fukuda, Y. Taguchi and M. Ogasa, "Basic Study of a Circuit Configuration for Power Transformer-less A.C. Fed Electric Trains using High Withstand Voltage Property of SiC Power Devices," *in IEEJ Transactions on Industry Applications,* vol. 139, no. 10, pp. 856–862, Oct. 2019.

[5] R. W. A. A. De Doncker, D. M. Divan and M. H. Kheraluwala, "A Three-Phase Soft-Switched High-Power-Density DC/DC Converter for High-Power Applications," *in IEEE Transactions on Industry Applications,* vol. 27, no. 1, pp. 63–73, Jan.-Feb. 1991.

[6] M. Leibl, G. Ortiz and J. W. Kolar, "Design and Experimental Analysis of a Medium-Frequency Transformer for Solid-State Transformer Applications," *in IEEE Journal of Emerging and Selected Topics in Power Electronics,* vol. 5, no. 1, pp. 110–123, Mar. 2017.

[7] N. H. Baars, J. Everts, H. Huisman, J. L. Duarte and E. A. Lomonova, "A 80-kW Isolated DC-DC Converter for Railway Applications," *in IEEE Transactions on Power Electronics,* vol. 30, no. 12, pp. 6639–6647, Dec. 2015.

[8] R. L. Steigerwald, "A Comparison of Half-Bridge Resonant Converter Topologies," *in IEEE Transactions on Power Electronics,* vol. 3, no. 2, pp. 174–182, Apr. 1988.

[9] D. Dujic, F. Kieferndorf, F. Canales and U. Drofenik, "Power Electronic Traction Transformer Technology," *Proceedings of The 7th International Power Electronics and Motion Control Conference,* pp. 636–642, 2012.

[10] M. Pavlovsky, S. W. H. de Haan and J. A. Ferreira, "Reaching High Power Density in Multikilowatt DC-DC Converters With Galvanic Isolation," *in IEEE Transactions on Power Electronics,* vol. 24, no. 3, pp. 603–612, Mar. 2009.

[11] C. Yao, X. Zhang, Y. Zhang, P. Yang, H. Li and J. Wang, "Semiconductor-Based Galvanic Isolation: Touch Current Suppression," *in IEEE Transactions on Power Electronics,* vol. 35, no. 1, pp. 48–58, Jan. 2020.

[12] Y. Hayashi, Y. Matsugaki and T. Ninomiya, "Capacitively Isolated Multicell dc-dc Transformer for Future dc Distribution System," *in IEEJ Journal of Industry Applications,* vol. 6, no. 4, pp. 268–277, Jul. 2017.